

Electronic Supplementary Information

Low-Bandgap Thieno[3,4-*c*]pyrrole-4,6-dione-Polymers for High-performance Solar Cells with Significantly Enhanced Photocurrents

Cheng Zhang,^a Hui Li,^a Jizheng Wang,^a Yongfang Zhang,^a Yan Qiao,^c Dazhen Huang,^a Chong-an Di,^a Xiaowei Zhan,^b Xiaozhang Zhu^{*a} and Daoben Zhu^a

^a Beijing National Laboratory for Molecular Sciences, CAS Key Laboratory of Organic Solids, Institute of Chemistry, Chinese Academy of Sciences, Beijing 100190, P. R. China.

^b Department of Materials Science and Engineering, College of Engineering, Peking University, Beijing 100871, P. R. China.

^c State Key Laboratory of Coal Conversion, Institute of Coal Chemistry, Chinese Academy of Sciences, Taiyuan, Shanxi Province, 030001, P. R. China.

* E-mail: xzzhu@iccas.ac.cn

Contents

Part 1. General information	S2
Part 2. Synthesis	S4
Part 3. Physical properties and thin-film morphology	S5
Part 4. Semiconducting properties	S10
Part 5. Solid-state 2D ¹³C{¹H} HETCOR NMR spectra	S12

Part 1. General information

Materials: All the reactions dealing with air- or moisture-sensitive compounds were carried out in a dry reaction vessel under a positive pressure of nitrogen. Unless stated otherwise, starting materials were obtained from Adamas, Aldrich and J&K and were used without any further purification. Anhydrous toluene was distilled over Na/benzophenone prior to use. Anhydrous DMF was distilled over CaH₂ prior to use. 1,3-bis(4-bromo-2-hexylthieno[3,4-*b*]thiophen-6-yl)-5-(2-ethylhexyl)-4*H*-thieno[3,4-*c*]pyrrole-4,6(5*H*)-dione (**TBTT_{EH-i}**),¹ 1,3-bis(6-bromo-2-hexylthieno[3,4-*b*]thiophen-4-yl)-5-(2-ethylhexyl)-4*H*-thieno[3,4-*c*]pyrrole-4,6(5*H*)-dione (**TBTT_{EH-o}**),¹ 1,3-bis(4-bromo-2-hexylthieno[3,4-*b*]thiophen-6-yl)-5-(2-hexyldecyl)-4*H*-thieno[3,4-*c*]pyrrole-4,6(5*H*)-dione (**TBTT_{HD-i}**)¹ and (4,8-bis(5-(2-ethylhexyl)thiophen-2-yl)benzo[1,2-*b*:4,5-*b'*]dithiophene-2,6-diyl)bis(trimethylstannane) (**BDT-Sn**)² were synthesized according to the procedure reported in the literatures.

General Methods: Elemental analyses were measured on a Carlo Erba 1106 elemental analyzer. Gel permeation chromatography (GPC) was performed on Polymer Laboratories PL-GPC220 at 150 °C using 1, 2, 4-trichlorobenzene (TCB) as eluent. UV-vis spectra were recorded on a JASCO V-570 spectrometer. Cyclic voltammetry (CV) measurements were carried out on a CHI640C analyzer in a conventional three-electrode cell setup with glassy-carbon electrode as the working electrode, a platinum wire as the counter electrode, Ag/Ag⁺ as the reference electrode and calibrated with ferrocene/ferrocenium (Fc/Fc⁺) as an external potential marker in anhydrous acetonitrile solution containing 0.1 M tetrabutylammonium perchlorate (TBAP) as a supporting electrolyte under a nitrogen atmosphere at room temperature. All potentials were corrected against Fc/Fc⁺. CV was measured with a scan rate of 100 mV/ s. Ultraviolet photoemission spectroscopy (UPS) was performed by on an AXIS ULTRA DLD with a He I (21.2 eV) source. Thermogravimetric analysis (TGA) was performed on a Shimadzu DTG 60 instrument at a heating rate of 10 °C min⁻¹ under a N₂ atmosphere with runs recorded from room temperature to 550 °C. DSC analyses were recorded on a Perkin Elmer Pyris 1 instrument under a dry N₂ flow at a heating rate of 10 °C min⁻¹, heating from room temperature to 300°C. X-Ray diffraction (XRD) measurements of thin films were performed in reflection mode at 40 kV and 200 mA with Cu K α radiation using a 2 kW Rigaku X-ray diffractometer. Atomic force microscopy (AFM) images of the thin films were obtained on a NanoscopeIIIa AFM (Digital Instruments) operating in tapping mode. Transmission electron microscopy (TEM) was performed using a JEOL 2200FS instrument at 160 kV accelerating voltage.

Computational Study: Density functional theory (DFT) (the B3LYP/6-31G** level of theory in vacuum) was utilized to model the structural and electronic properties of relevant molecular structures. The alkyl chains were replaced by methyl groups to keep the computational time within a reasonable range.

Fabrication of polymer solar cells: Polymer solar cell devices were fabricated using ITO-coated glass substrates ($15 \Omega \text{ sq}^{-1}$), which were cleaned with de-ionized water, acetone, and isopropyl alcohol in successive 25 min sonication steps applying a final 6 min oxygen plasma treatment to eliminate any remaining organic component. In the conventional structure devices, a thin layer (ca. 30 nm) of PEDOT:PSS (Bayer Baytron 4083) was first spin-coated on the pre-cleaned ITO-coated glass substrates at 2000 rpm and baked at 150°C for 15 min under ambient conditions. The substrates were then transferred into a nitrogen-filled glove box. Subsequently, the active layer was spin-coated on the PEDOT:PSS layer by spin-coating from a 10 mg/ml *o*-dichlorobenzene solution of polymer and PC₇₁BM. Solvent additive, 1,8-diiodooctane (DIO), and annealing were used to improve the BHJ morphology. At the final stage, the substrates were pumped down in high vacuum, and calcium (20 nm) topped with aluminium (80 nm) was thermally evaporated onto the active layer. For inverted device fabrication, a thin layer of sol-gel ZnO (ca. 30 nm) was spin-coated onto precleaned ITO-coated glass substrates at 2000 rpm and then annealed at 200°C for 1h in air. The ZnO precursor solution was prepared by dissolving zinc acetate dehydrate $\text{C}_4\text{H}_6\text{O}_4\text{Zn}\cdot 2(\text{H}_2\text{O})$ (99.5%, Merck 1 g) and monoethanolamine ($\text{HOCH}_2\text{CH}_2\text{NH}_2$, 98% Acros, 0.28 g) in 2-methoxyethanol ($\text{CH}_3\text{OCH}_2\text{CH}_2\text{OH}$, Aldrich, 98%, 10 mL) under stirring for 8 h for hydrolysis reaction and aging. The same process used for active layer in the conventional structure devices was also used for the inverted devices. After that, a 3 nm thick MoO_3 film and 80 nm Ag were deposited to complete the inverted device structure. Shadow masks were used to define the OSC active area (0.044 cm^2) of the devices.

Device Characterization: The current density–voltage (J – V) characteristics of unencapsulated photovoltaic devices were measured under N_2 using a Keithley 2400 source meter. A 300 W xenon arc solar simulator (Oriel) with an AM 1.5 global filter operated at 100 mW cm^{-2} was used to simulate the AM 1.5G solar irradiation. The illumination intensity was corrected by using a silicon photodiode with a protective KG5 filter calibrated by the National Renewable Energy Laboratory (NREL). The external quantum efficiency (EQE) was performed using certified IPCE equipment (Zolix Instruments, Inc, SolarCellScan100).

OTFT Device fabrication and measurements: A heavily doped Si wafer with a 300 nm SiO_2 served as the gate electrode and dielectric layer, respectively. 30 nm Au electrodes were deposited and patterned by a typical lift-off technique with channel length ranging from 5–50 μm and channel width of 1.4 mm. The OTS modification was carried out in a vacuum oven at a temperature of 120°C for 3 hours. The treated substrates were rinsed successively with hexane, ethanol and chloroform, respectively. The organic active layer was deposited on the OTS-treated substrates by a spin-coating process of their *o*-dichlorobenzene solutions, which followed by the annealing treatments at varied temperatures.

SCLC Mobility Measurements: Space charge-limited currents were tested in electron-only devices with a configuration of glass/Al/polymer:PC₇₁BM/Al and hole-only devices with a configuration of

ITO/PEDOT:PSS/polymer:PC₇₁BM/Au. The devices were prepared following the same procedure described in the experimental section for photovoltaic devices, except for the metal electrode. The mobilities were determined by fitting the dark current to the model of a single carrier SCLC current with field dependent mobility, which is described as

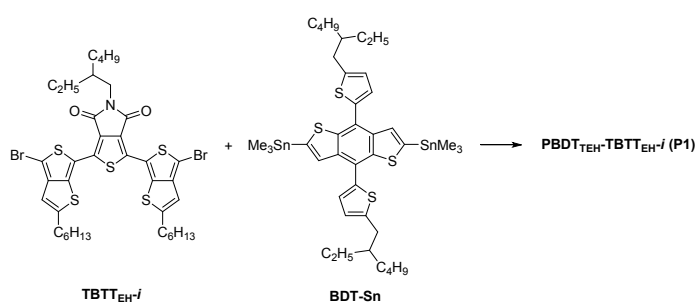
$$J = \frac{9\varepsilon_0\varepsilon_r\mu_0V^2}{8L^3} \quad (1)$$

Where J is the current, μ_0 is the zero-field mobility, ε_0 is the permittivity of free space, ε_r is the relative permittivity of the material, V is the effective voltage, and L is the thickness of the active layer.

Solid-state 2D ¹³C{¹H} HETCOR NMR experiments were performed on 600MHz Bruker Avance III spectrometer operating at a resonance frequency of 600.48 MHz for ¹H and 151.00 MHz for ¹³C. The experiments were conducted on a Bruker 4-mm double-resonance MAS probe at room temperature with the MAS speed at 10 kHz. Cross-polarization (CP) was used to transfer magnetization from ¹H to ¹³C nuclei according to the Hartmann-Hahn condition. The 1D ¹³C CP-MAS experiments utilized a contact time of 2 ms. The 1D CP pulse sequence implemented a ramped (50 to 100 %) spin-lock pulse on the ¹H channel and a square contact pulse on the ¹³C channel. Heteronuclear ¹H decoupling was applied during signal acquisition using the SPINAL-64 pulse sequence at a ¹H decoupling field of 80 kHz. The HETCOR experiments performed with CP contact times of 0.4 ms. A total of 256 t1 increments with 384 scans were collected. The chemical shift of ¹H was referenced to tetramethylsilane (TMS, 0 ppm) and ¹³C was referenced to methylene carbon of adamantane at 38.48 ppm.

Part 2. Synthesis

Polymerization for PBDT-TBTTs



PBDT_{TEH}-TBTT_{EH-i} (P1)

TBTT_{EH-i} (102 mg, 0.117 mmol) and BDT-Sn (115 mg, 0.127 mmol) were dissolved with toluene (2 ml) and DMF (1 ml) in a pressure-proof tube. The reaction container was purged with argon for 10 min, and then Pd(PPh₃)₄ (10 mg, 0.008 mmol) was added. After another flushing with argon for 15 min, the reactant was heated to 100 °C for 36 h in dark. The reaction mixture was cooled to room temperature and poured into MeOH (80 mL), and filtered, which was then subjected to Soxhlet extraction with methanol, hexane, and chloroform successively. The polymer was recovered from the chloroform

fraction by precipitation with methanol. The dark red solid was dried under vacuum to give 120 mg of **P1** in 80% yield. GPC: $M_w = 33.3$ K; $M_n = 7.9$ K; PDI = 4.21. Anal. Calcd for $C_{72}H_{87}NO_2S_9$ (%): C, 67.19; H, 6.81; N, 1.09; Found (%): C, 66.56; H, 6.72; N, 1.10.

PBDT_{TEH}-TBTT_{EH-o} (**P2**)

P2 was synthesized following the same procedure as **P1** starting from TBTT_{EH-o} (150 mg, 0.17 mmol), BDT-Sn (169 mg, 0.187 mmol) and Pd(PPh₃)₄ (14 mg, 0.012 mmol). **P2** was recovered from the chloroform fraction by precipitation with methanol. The dark red solid was dried under vacuum to give 142 mg of **P2** in 64% yield. GPC: $M_w = 22.0$ K; $M_n = 5.5$ K; PDI = 3.98. Anal. Calcd for $C_{72}H_{87}NO_2S_9$ (%): C, 67.19; H, 6.81; N, 1.09; Found (%): C, 66.24; H, 6.71; N, 1.13.

PBDT_{TEH}-TBTT_{HD-i} (**P3**)

P3 was synthesized following the same procedure as **P1** starting from TBTT_{HD-i} (100 mg, 0.102 mmol), BDT-Sn (100 mg, 0.110 mmol) and Pd(PPh₃)₄ (8 mg, 0.007 mmol). The polymer was recovered from the chlorobenzene fraction by precipitation with methanol. The dark red solid was dried under vacuum to get 125 mg of **P3** in 88% yield. GPC: $M_w = 22.9$ K; $M_n = 6.1$ K; PDI = 3.77. Anal. Calcd for $C_{80}H_{103}NO_2S_9$ (%): C, 68.67; H, 7.42; N, 1.00; Found (%): C, 68.95; H, 7.15; N, 0.98.

Part 3. Physical properties

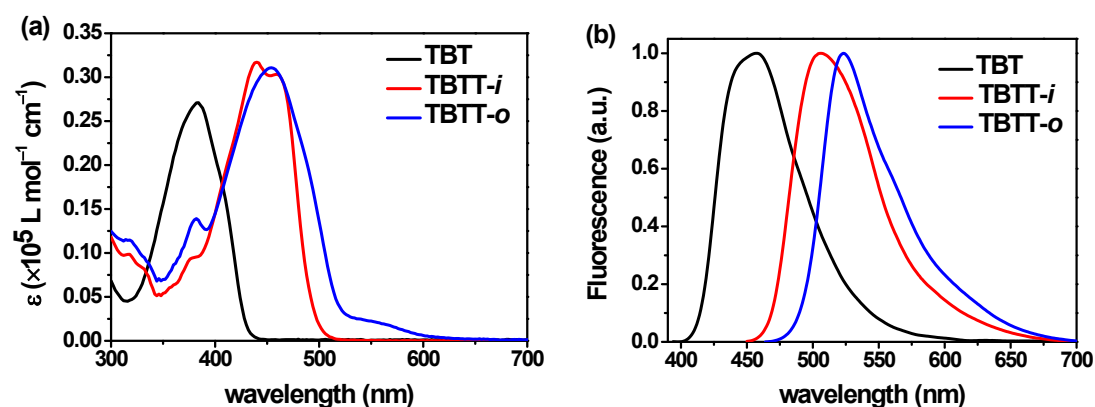


Figure S1. UV-Vis absorption spectra (a) and fluorescence spectra (b) of TBT, TBTT-*i* and TBTT-*o* in diluted CH₂Cl₂ solution (1×10^{-5} M).

Table S1. Photophysical properties of TBT, TBTT-*i* and TBTT-*o* in dilute CH₂Cl₂ solution.

Cpd.	$\lambda_{\text{abs}}^{\text{max}}$ (nm)	ϵ_{max} (L mol ⁻¹ cm ⁻¹)	$\lambda_{\text{max}}^{\text{em}}$ (nm)	Stokes shift (cm ⁻¹)	E_g^{opt} (eV) ^{a)}
TBT	384	27100	457	4160	2.88
TBTT- <i>i</i>	440, 460	31700	506	1976	2.48

a) The optical bandgap was calculated according to $E_g^{\text{opt}} = 1240/\lambda_{\text{onset}}$, where λ_{onset} is the onset value of the absorption spectrum in the long wavelength region.

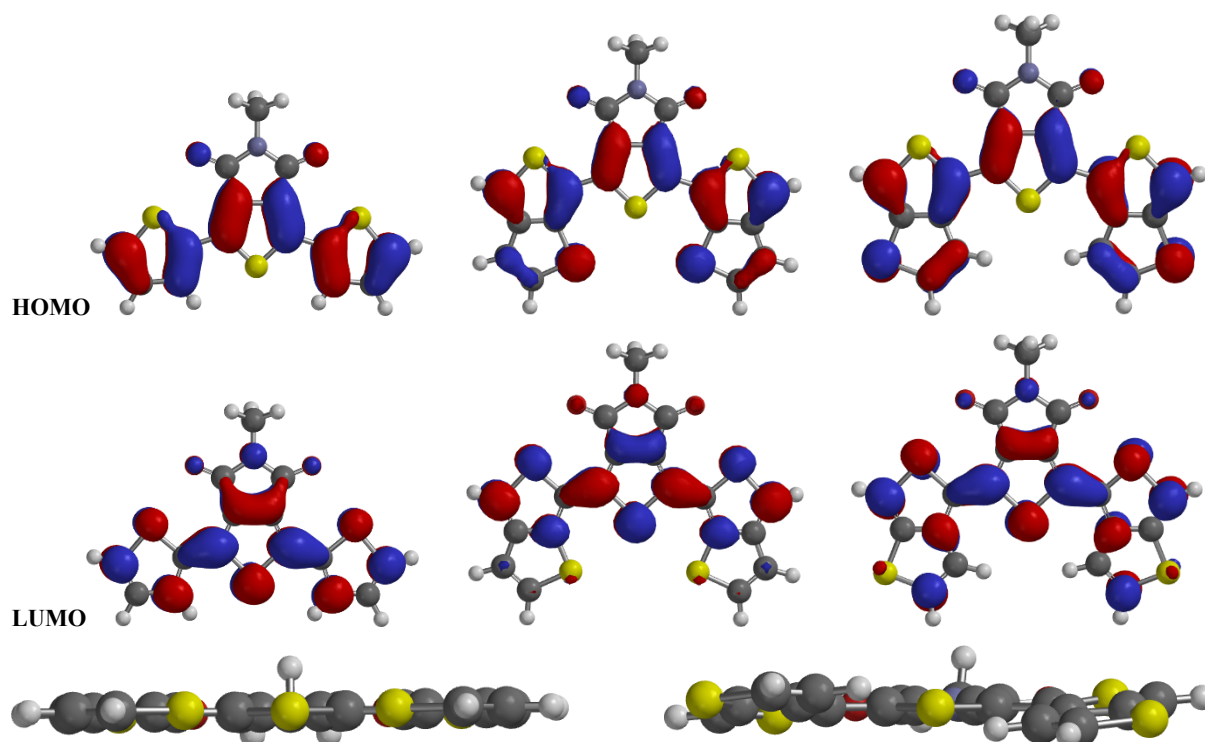


Figure S2. (up) Calculated HOMO and LUMO orbitals of TBT, TBTT-*i*, and TBTT-*o*. Alkyl substituents are replaced by methyl groups to simplify the calculations. (down) Projected view of TBTT-*i* and TBTT-*o* from the short-axis direction.

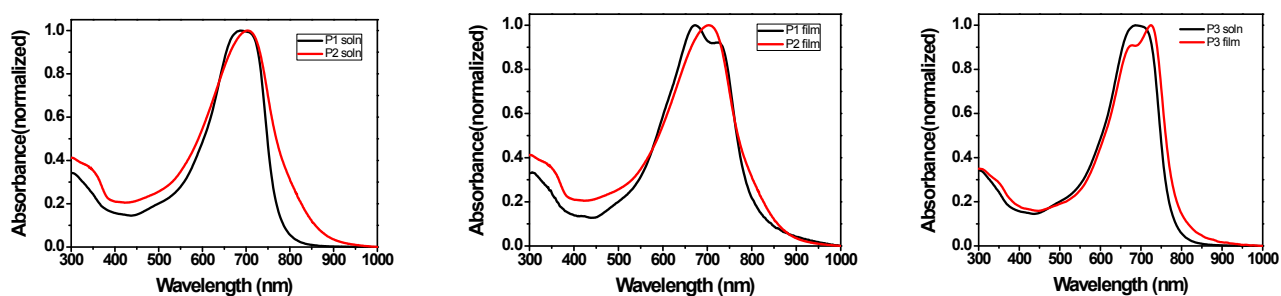


Figure S3. The UV-vis spectra of P1 and P2 in chloroform (left) and thin film (middle) and P3 in chlorobenzene and thin film (right).

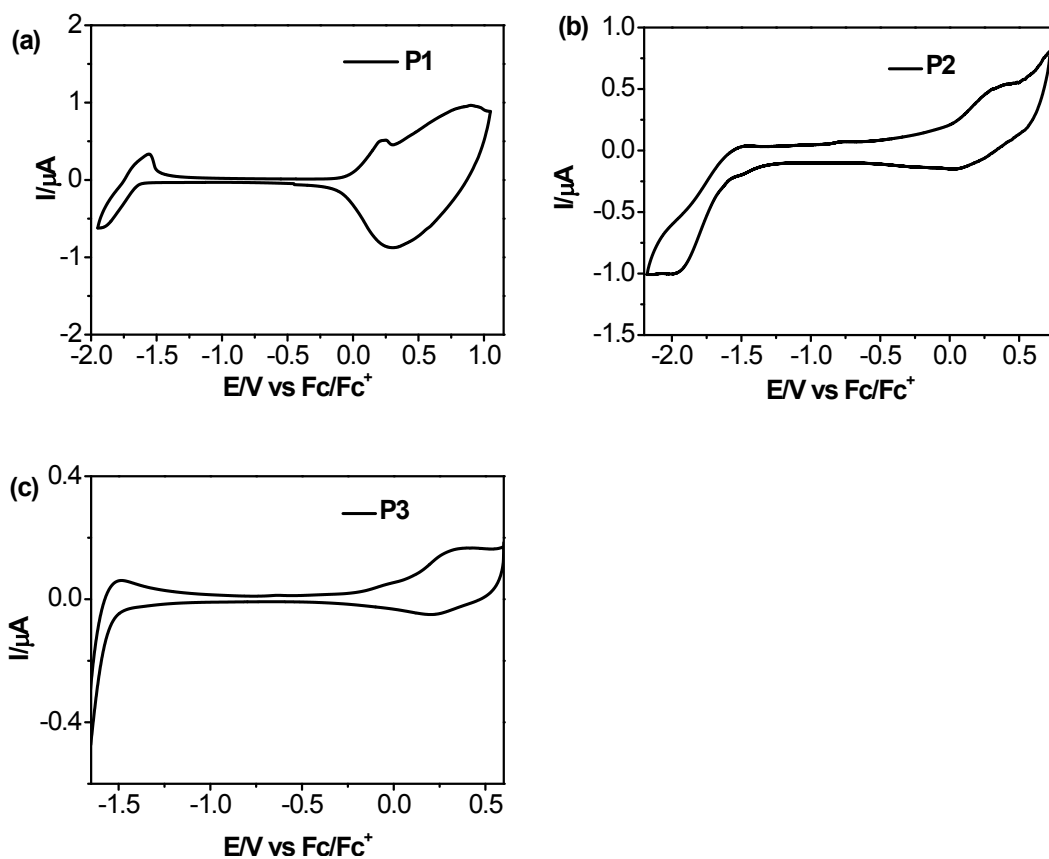


Figure S4. Cyclic voltammogram of (a) **P1**, (b) **P2** and (c) **P3** films on the glassy-carbon electrode with scan rate of 100 mV s^{-1} .

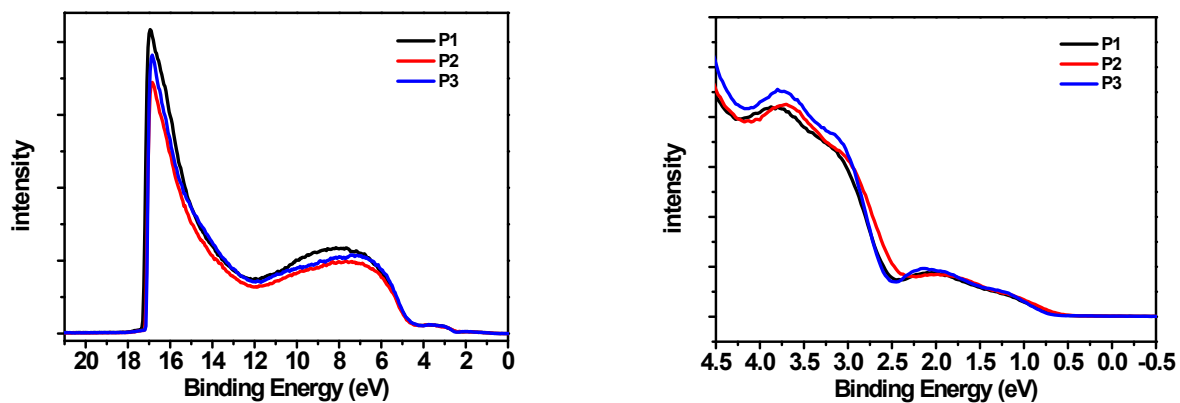
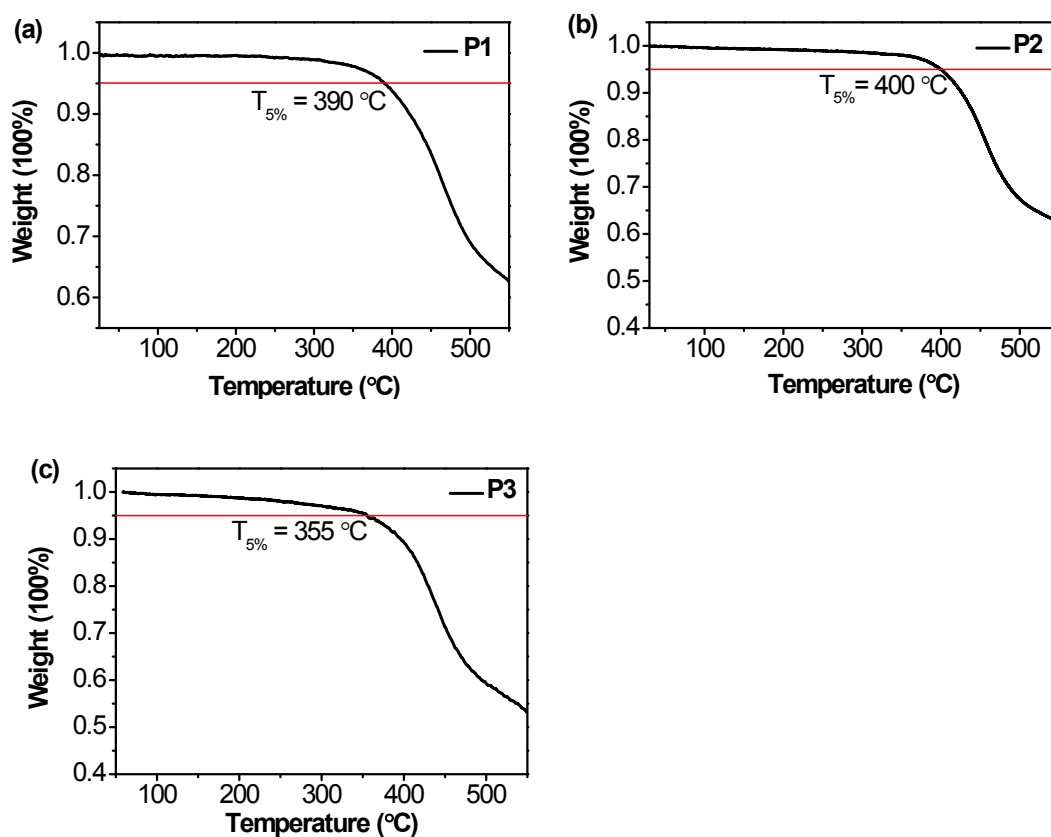


Figure S5. Ultraviolet photoelectron spectroscopy (UPS) of **P1-P3** films on Si substrate.

Table S2. Photo physical and electrochemical properties of **P1**, **P2** and **P3** in solution and films

Polymers	$\lambda_{\max}^{\text{soln}}$ (nm)	$\lambda_{\max}^{\text{film}}$ (nm)	E_g^{film} (eV) ^{a)}	HOMO ^{CV} (eV) ^{b)}	LUMO ^{CV} (eV) ^{c)}	HOMO ^{UPS} (eV) ^{d)}	LUMO ^{UPS} (eV) ^{e)}
P1	686	672,726	1.54	-5.12	-3.58	-4.64	-3.10
P2	704	706	1.46	-5.12	-3.66	-4.63	-3.17
P3	688	678,724	1.56	-5.12	-3.56	-4.78	-3.22

a) The optical bandgap was calculated according to $E_g^{\text{film}} = 1240/\lambda_{\text{onset}}$ (eV), where λ_{onset} is the onset value of the absorption spectrum in the long wavelength region; b) Estimated from the empirical equation $\text{HOMO}^{\text{CV}} = -(5.10 + E_{\text{onset}})$ (eV); c) Determined from the empirical equation $\text{LUMO}^{\text{CV/UPS}} = \text{HOMO}^{\text{CV/UPS}} + E_g^{\text{film}}$ (eV); d) Estimated from the empirical equation $\text{HOMO}^{\text{UPS}} = \text{WF} + E_b$ (eV), where WF is the d-value between 21.22 and the onset value of the high binding energy, E_b is the onset value of the low binding energy.

**Figure S6.** Thermal gravimetric analysis (TGA) curves of polymers (a) **P1**, (b) **P2**, and (c) **P3**.

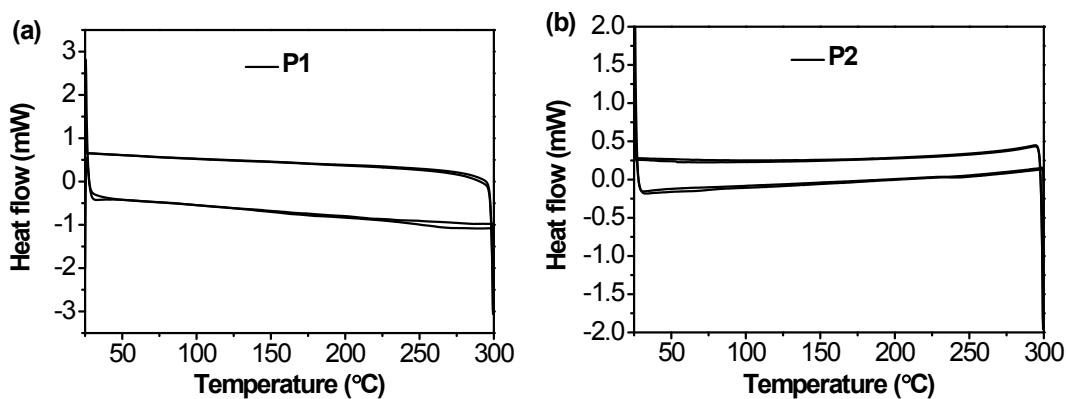


Figure S7. Differential scanning calorimetry (DSC) curves of powders of **P1** and **P2**. Upward peaks indicate exothermic processes, while downward peaks indicate endothermic processes.

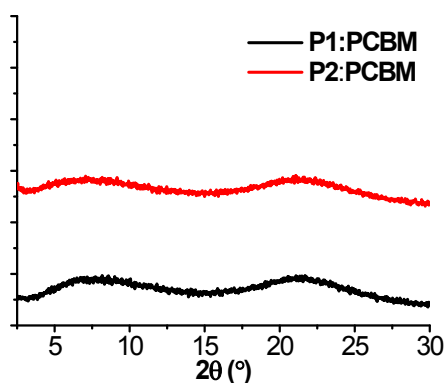


Figure S8. X-ray diffraction (XRD) patterns of polymer:PC₇₁BM optimized blend films.

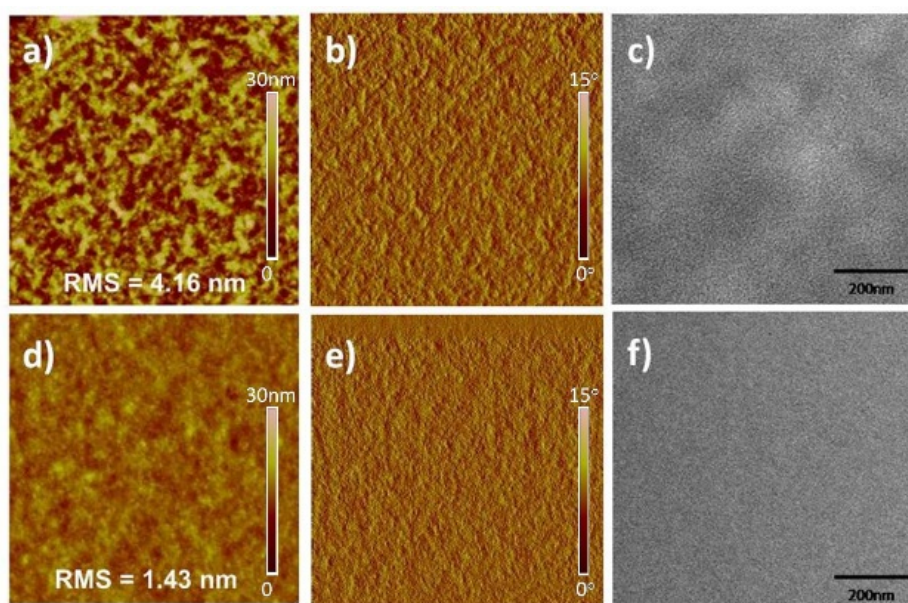


Figure S9 AFM height images (a, d), AFM phase images (b, e), and TEM images of optimized blend films (c, f) based on **P1**:PC₇₁BM (a–c) and **P2**:PC₇₁BM (d–e) blend films. The scan size of the AFM images is $5 \times 5 \mu\text{m}$.

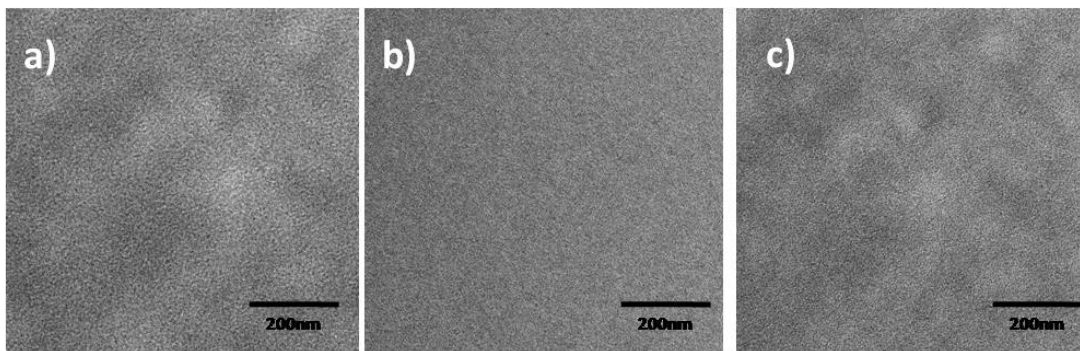


Figure S10. TEM images of (a) P1:PC₇₁BM, (b) P2:PC₇₁BM, and (c) P3:PC₇₁BM optimized blend films.

Part 4. Semiconducting properties

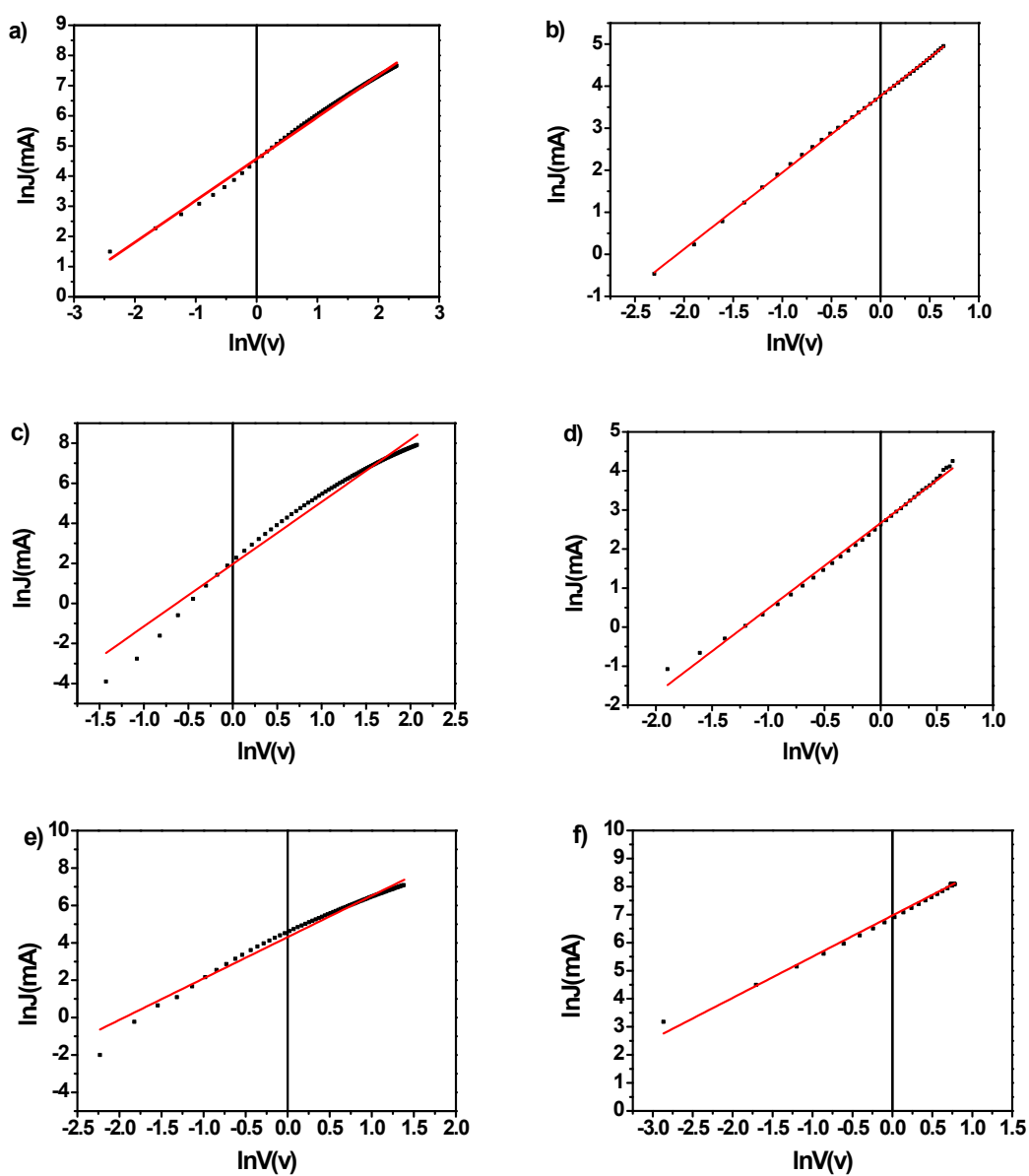


Figure S11. The hole mobility (a) and electron mobility (b) of **P1**:PC₇₁BM, the hole mobility (c) and electron mobility (d) of **P2**:PC₇₁BM blend films, the hole mobility (e) and electron mobility (f) of **P3**:PC₇₁BM blend films at their best OSC device characters measured by SCLC method.

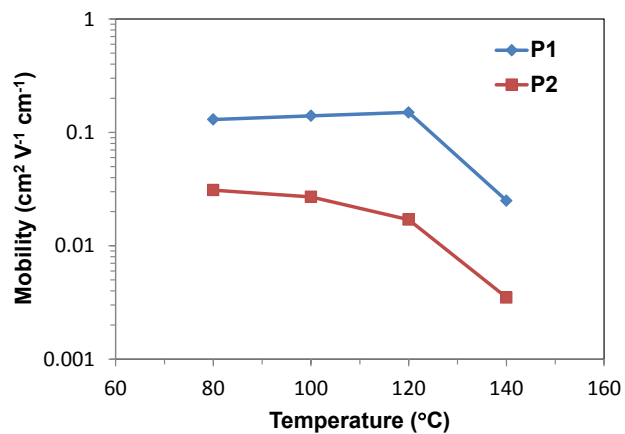


Figure S12. Comparison of the hole mobilities (OFET) of **P1** and **P2** at different annealing temperatures.

Figure S13. Solid-state 2D $^{13}\text{C}\{^1\text{H}\}$ dipolar-mediated heteronuclear correlation (HETCOR) NMR spectra acquired at room temperature for neat **P1** (a) and PC₆₁BM (b) Solid-state 2D $^{13}\text{C}\{^1\text{H}\}$ dipolar-mediated heteronuclear correlation (HETCOR) NMR spectra acquired at room temperature for mixture contains 8 wt.% **P1** and 92 wt% PC₆₁BM. (c) Diagrammatic sketch that indicate the most probable arrangement of **P1** and PC₆₁BM according to the intermolecular interactions between them from the 2D NMR intensity correlations.

As shown in Figure S13, the mixture sample (Figure S13(c)), 8% polymer:92% PC₆₁BM by wt., were prepared by stirring approximately 150 mg of the material blend in *o*-DCB (20 mg/mL) overnight at room temperature. The solvent was removed under reduced pressure before being loaded into 4 mm zirconia rotors for measurement, while neat chemicals were loaded without processing. Because of the aggregation, the peaks in the polymer NMR spectrum (Figure S13(a)) are broadened, which are different from the relative sharp signals in the PC₆₁BM NMR spectrum (Figure S13(b)). Compared to the 2D $^{13}\text{C}\{^1\text{H}\}$ HETCOR NMR of PC₆₁BM and **P1**, additional 2D intensity correlations are observed in Figure S13(c) that directly establishes intermolecular interactions between the PC₆₁BM and **P1**. The ^{13}C signals at 24 and 34 ppm that are associated with C3' and C2' of the PC₆₁BM moiety are strongly correlated with the ^1H signals at ~7.5 ppm from H2 (BDT moiety) of **P1**. Meanwhile, the ^{13}C signal at 31 ppm and 51 ppm that are associated with C4' and C6' of the PC₆₁BM moiety are both correlated with the ^1H signals at ~7.5 ppm from H2 (BDT moiety) of **P1**, too. Moreover, ^{13}C signals associated with the C₆₀ fullerene group at 145–148 ppm are strongly correlated with the ^1H signals at 3.0~3.5 ppm associated with the alkyl chain of TPD. These results are also in good agreement with a recently published paper,³ in which the alkoxy units on BDT have steric hindrance to push the PC₆₁BM to the TPDs. Thus, the thiophene substituents on BDT in **P1–P3** should have greater steric hindrance.

Reference

- 1 C. Zhang, Y. Zang, E. Gann, C. R. McNeill, X. Zhu, C.-a. Di, D. Zhu, *J. Am. Chem. Soc.*, 2014, **136**, 16176.
- 2 P. Liu, K. Zhang, F. Liu, Y. Jin, S. Liu, T. P. Russell, H.-L. Yip, F. Huang, Y. Cao, *Chem. Mater.*, 2014, **26**, 3009.
- 3 K. Graham, C. Cabanetos, J. P. Jahnke, M. N. Idso, A. E. Labban, G. O. N. Ndjawa, T. Heumueller, K. Vandewal, A. Salleo, B. F. Chmelka, A. Amassian, P. M. Beaujuge, M. D. McGehee, *J. Am. Chem. Soc.*, 2014, **136**, 9608.